Nuclear Data for Science and Technology (1988 MITO), 561- 564, Copyright © 1988 JAERI.

STUDY ON APPLICABILITY OF GLOBAL NEUTRON OPTICAL MODEL POTENTIALS TO A NUCLEAR MASS RANGE FROM SODIUM TO GOLD AND TO ENERGIES FROM 1 TO 50 MeV

Hisao Yamakoshi

Ship Research Institute
6-38-1 Shinkawa, Mitaka, Tokyo 181, Japan

Absstract: Applicability of neutron optical model potentials was studied by comparing calculated results with experimental data on σ_t, σ_{non}, $d\sigma_{el}/d\Omega$, the s-wave and the p-wave neutron strength functions: S_0 and S_1, and the potential scattering radii R' for isotopes and elements in a wide mass range from sodium to gold. The quantities S_0, S_1 and R' were calculated at 10 keV; the quantities σ_t, σ_{non} (or σ_{comp}) and $d\sigma_{el}/d\Omega$ were calculated in a wide energy range from about 1 MeV to 50 MeV. The neutron OMPs considered in the present study were those potentials reported by Becchetti and Greenlees, Hilmore and Hodgson, Rapaport et. al., and by the author. In the comparison, results of other author's analyses were taken into account as reference data. Conclusions are : (1) the potential by Wilmore and Hodgson has a tendency of overestimating the total cross section near 50 MeV, (2) the potential by Rapaport has a tendency of underestimating the total cross section near 50 MeV, (3) the Rapaport's potential seems to underestimate the nonelastic cross sections of nuclei with large mass numbers such as ^{181}Ta and ^{197}Au. (4) the potential by the author seems to be more advantageous as a global potential than the other potentials considered in the present study.

(neutron, optical model potential, global, applicability, 50 MeV, σ_t, σ_{non}, $d\sigma_{el}/d\Omega$)

Introduction

The present applicability study stems from the view point that a good global neutron OMP is worthy of finding for the purpose of keeping a consistency among neutron nuclear data predicted for those nuclei of which experimental nuclear data are not available.

The Becchetti-Greenlees potential[1] and the Hilmore-Hodgson potential[2] were adopted as well known potentials. As hopeful potentials, both Rapaport potential[3] and the author's potential[4] were also considered in the present study.

The quantities σ_t, $d\sigma_{el}/d\Omega$ and σ_{comp} were calculated with ELIESE-3 code[5] as well as the quantities S_0, S_1 and R'. In the calculation of σ_{non}, GNASH code[6] was utilized. Although the main purpose of the present study is the applicability of these potentials to the larger energy region from 1 MeV to 50 MeV, behavior of these potentials in lower energy region was also taken into account by calculating S_0, S_1 and R' at 10 keV as well as σ_t bellow 1 MeV.

Optical Model Potentials Adopted

The potential parameters for the adopted OMPs are tabulated in Table 1. The potential reported by the author is referred to the Yamakoshi potential for convenience of later discussion. The imaginary surface part of this potential has the Gaussian form, while the others have the derivative Woods-Saxon form for their imaginary surface terms. In the case of the Rapaport potential, the parameter set A in his report was chosen because this set is adopted in the Hansen's optical potential analysis[7].

Comparison

σ_t

Calculated total cross sections for ^{27}Al, Cu, ^{181}Ta and ^{197}Au are compared with the experimental data in Figs.1 through 4. In the case of Cu, the result of coupled channel analysis by Delaroche et. al.[8] is also compared as reference data. The Yamakoshi potential yields very close result to the Delaroche's result. As a typical example, the Hilmore-Hodgson potential overestimates the total cross section of Cu near 50 MeV. Similar tendency can be seen in the case of ^{27}Al. For the neutron energies lower than 1 MeV, the Yamakoshi potential seems to be in better agreement with experimental data than the other potentials.

σ_{non}

The nonelastic cross section σ_{non} can be calculated by subtracting the calculated compound elastic part from the calculated compound nucleus formation cross section σ_{comp} as shown in Fig.5 where σ_{non} for sodium is calculated by using the Yamakoshi potential. Consequently, calculated σ_{comp} should not be less than the experimental data of σ_{non} if the calculated σ_{non} is in good agreement with the experimental data of σ_{non}. As seen in Figs.6 and 7, the calculated σ_{comp} values are certainly larger than or equal to the measured σ_{non} data. However, for eavy nuclei such as ^{181}Ta and ^{197}Au, the values of σ_{comp} calculated by using the Rapaport potential are smaller than the measured data of σ_{non} in some neutron energy range as seen in Figs.8 and 9.

$d\sigma_{el}/d\Omega$

Calculated results for the case of En = 14.6 MeV are compared with experimental data in Fig.10 for six isotopes. Results of analysis by Hansen et. al. with potential reported by Breiva et. al.[9] and with the potential reported by Jeukenne et. al.[10] are also compared in this figure. In the case of small scattering angle, results by the Yamakoshi potential are very close to those with the Jeukenne potential which is refered to as JLM in this figure.

Incident energy dependence of the calculated results is compared with that of measured data in Fig.11 for the case of ^{63}Cu. Results of the coupled channel analysis by Delaroche et. al. are also compared in this figure. For scattering angles near 0 degrees, Delaroche's results are very close to the results with Yamakoshi potential rather than those with other OMPs.

R', S_0 and S_1

Calculated results of R', S_0 and S_1 are compared with experimental results in Figs. 12 through 14. The Rapaport potential seems to enhance the mass number dependences of experimental results for these quantities. Especially, around A = 180, R' and S_0 calculated with this potential seems to be too large in comparison with the experimental data.

Discussions

Judging from the comparison of σ_t between calculation and measurement near 50 MeV for aluminum and copper, the Wilmore-Hodgson potential seems to overestimate the total cross sections of other nuclei around 50 MeV. On the other hand, the Rapaport potential seems to under estimate the total cross sections around 50 MeV.

The underestimation of σ_{comp} for ^{181}Ta and ^{197}Au by using the Rapaport potential may be an evidence that this potential is not applicable to nuclei with nuclear mass number as large as gold.

The Becchetti-Greenlees potential seems to overestimate a bit the higher energy part of the nonelastic cross section. However, this overestimation can be large eneough to cause a large amount of over estimation in cross sections for reactions such as (n,n'), (n,2n), (n,p) and (n,α).

The Yamakoshi Potential has ever been applied to the analyses of both sodium and iron nuclear data for JENDL-3. From the experience of the application, this potential is thought to be a good potential for nuclei from sodium to iron. It may be said as a result of the present study that one can apply this potential to nuclei as heavy as gold.

Conclusions

As a summary, following conclusions are derived:

(1) The Wilmore-Hodgson potential has a tendency of overestimating the total cross section near 50 MeV.

(2) The Rapaport potential underestimates very much the values of neutron nonelastic cross section of ^{181}Ta and ^{197}Au.

(3) The Yamakoshi potential seems to be more advantageous as a global potential than the other potentials considered in the present study.

REFERENCES

1. F.D.Becchetti,Jr, and G.W.Greenlees: Phys. Rev. 182, 1190 (1969)
2. D.Wilmore and P.E.Hodgson: Nucl. Phys. 55, 673 (1964)
3. J.Rapaport et. al.: Nucl. Phys. A330, 15 (1979)
4. H.Yamakoshi: JAERI-M 5984, 159 (1975)
5. S.Igarashi: JAERI 1224, 1 (1972)
6. P.G.Young and A.D.Arther: GNASH, LA-6974 (1977)
7. Hansen et. al.: Phys. Rev. C31, 111 (1985)
8. J.P.Delaroche et.al.: Nucl. Phys. A390, 541 (1982)
9. F.A.Brieva and J.R.Rook: Nucl. Phys. A291, 299 (1977), A291, 317 (1977)
10. J.P.Jeukenne et. al.: Phys. Rev. C16, 80 (1977)

Table 1. Potential Parameters for Adopted OMPs

			Becchetti-Greenlees	Wilmore-Hodgson	Rapaport	Yamakoshi **
Volume	Real Part	V	56.3 - 0.32E - 24§†	47.01 + 0.267E - 0.008E²	54.19 - 0.33E -(22.7 - 0.19E)§	46 - 0.33E
		r_0	1.17	r_0^*	1.198	1.286
		a_0	0.75	0.66	0.663	0.62
	Imaginary Part	W	-1.56 + 0.22E, or 0, which ever greater	-	0.0 ; E < 15 MeV, -4.3 + 0.38E ; E > 15 MeV.	$0.125E - 4\times10^{-4}E^2$
		r_w	1.26	-	1.295	1.286
		a_w	0.58	-	0.59	0.62
Surface Imaginary Part		W_D	13 - 0.25E - 12§, or 0, which ever greater	9.52 - 0.053E	4.28 + 0.4E -12.8§; E<15MeV, 14 - 0.39E -10.4§; E>15 MeV.	14 - 0.2E
		r_D	1.26	r_D^*	1.295	1.390
		a_D	0.58	0.48	0.59	0.7
Spin Orbital Part		V_{so}	6.2	-	6.2	6.0
		r_{so}	1.01	-	1.01	1.07
		a_{so}	0.75	-	0.75	0.62

$r_0^* = 1.322 - 7.6A\times10^{-4} + 4A^2\times10^{-6} - 8A^3\times10^{-9}$,
$r_D^* = 1.266 - 3.7A\times10^{-4} + 2A^2\times10^{-6} - 4A^3\times10^{-9}$,
† § ≡ (N - Z)/A
** Surface imaginary part has Gaussian form.

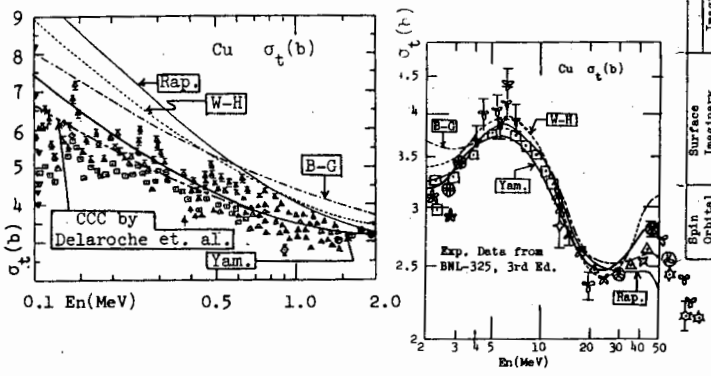

Fig. 1 Comparison of calculated total cross sections for Cu with experimental data

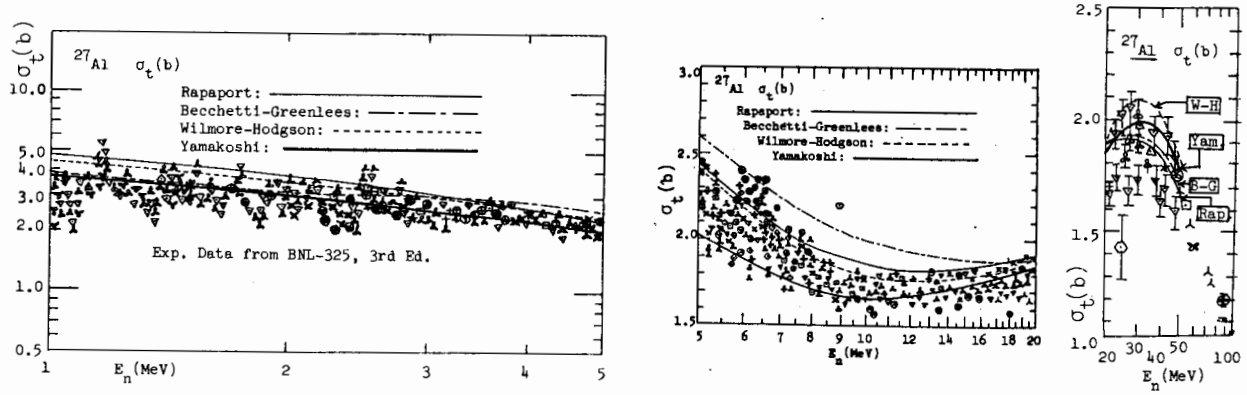

Fig.2 Comparison of calculated total cross sections for ^{27}Al with experimental data

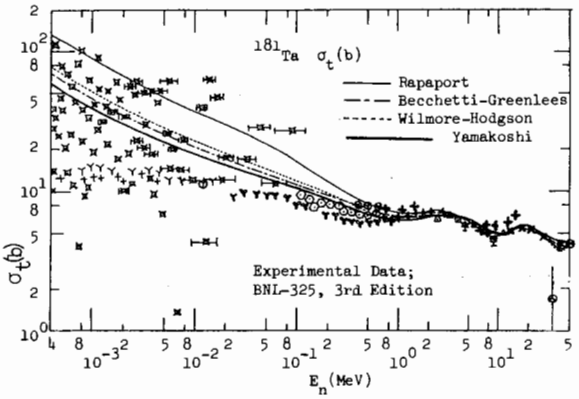

Fig.3 Comparison of calculated total cross sections for ^{181}Ta with experimental data

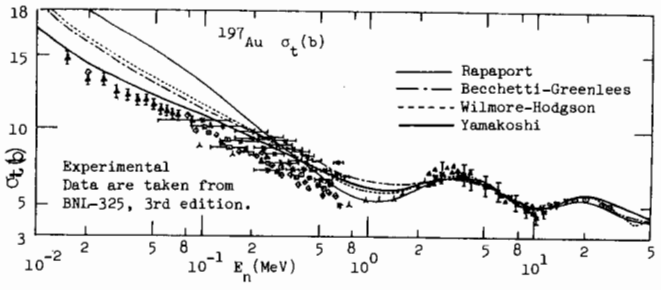

Fig.4 Comparison of calculated total cross sections for ^{197}Au with experimental data

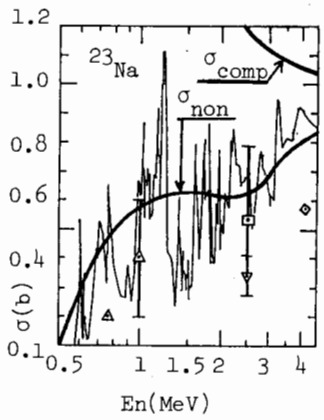

Fig.5 σ_{non} and σ_{comp} for ^{23}Na calculated with the Yamakoshi potential

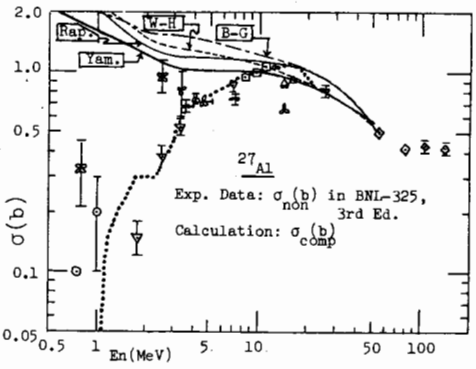

Fig.6 Comparison of calculated cross sections of σ_{comp} for ^{27}Al with experimental cross section data of σ_{non}

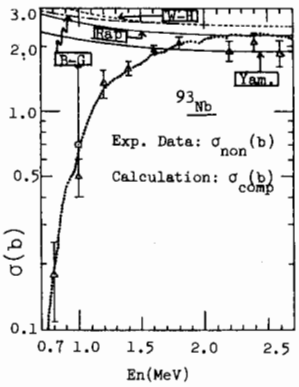

Fig.7 Comparison of calculated σ_{comp} cross sections for ^{93}Nb with experimental cross section data of σ_{non}

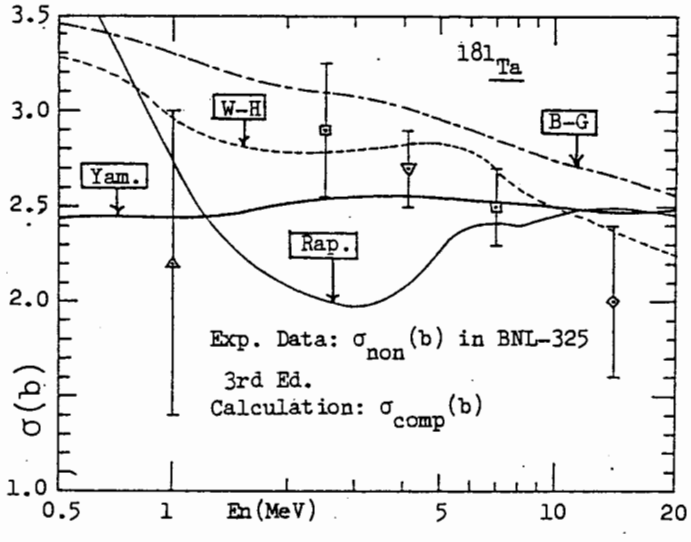

Fig.8 Comparison of calculated cross sections of σ_{comp} for ^{181}Ta with experimental cross section data of σ_{non}

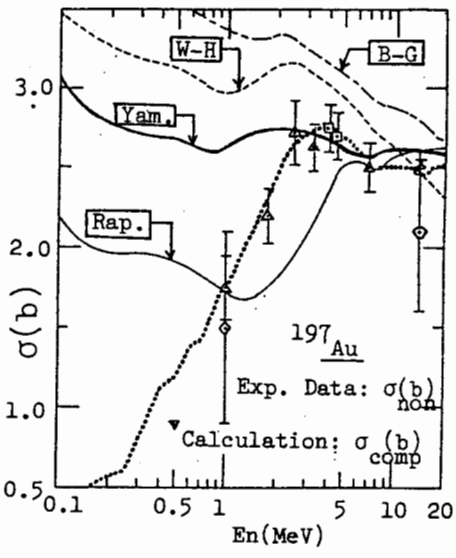

Fig.9 Comparison of calculated cross sections of ^{197}Au with experimental cross section data of σ_{non}

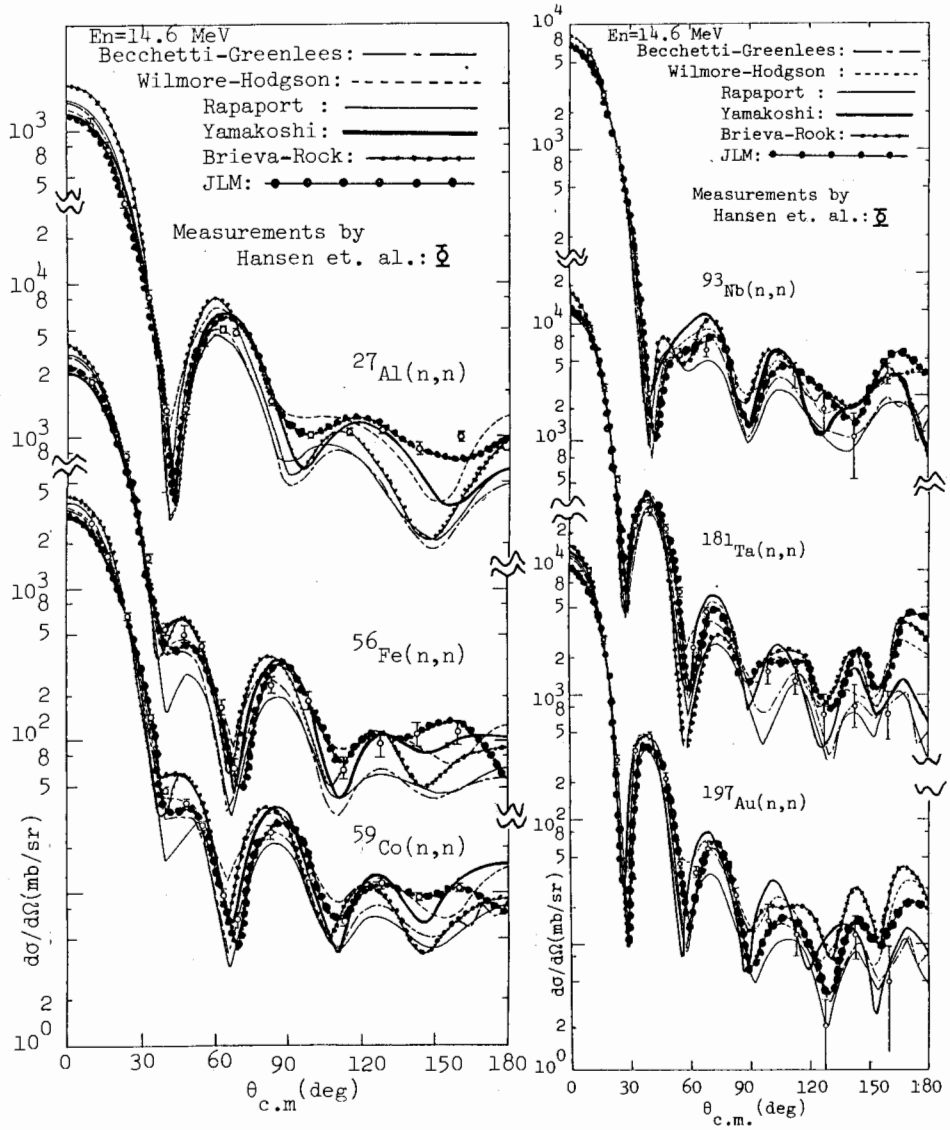

Fig.10 Comparison of calculated $d\sigma_{el}/d\Omega$ at En = 14.6 MeV with experimental data for several isotopes in a wide mass range

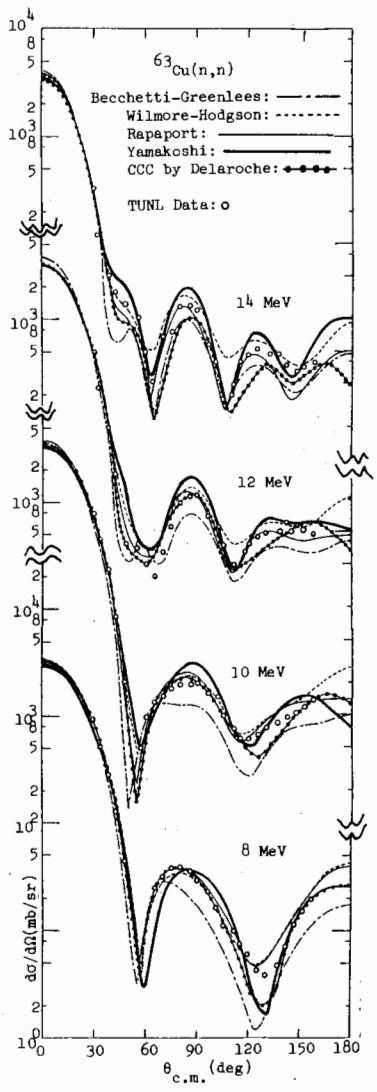

Fig.11 Comparison of $d\sigma_{el}/d\Omega$ for Cu between calculation and experiment

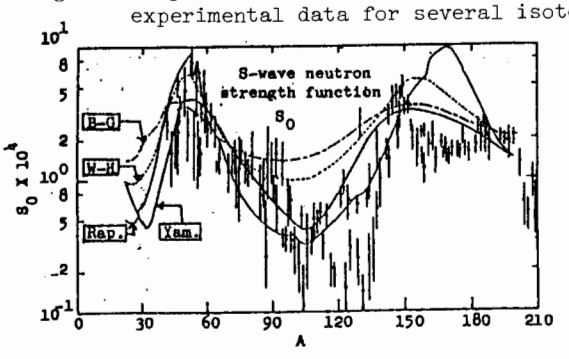

Fig.12 Intercomparison of S_0

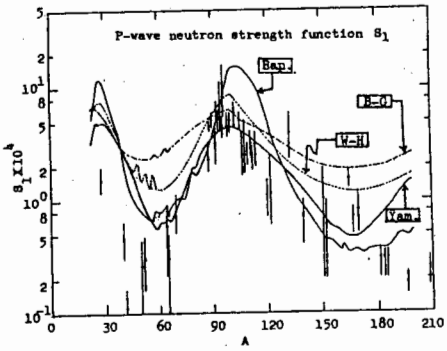

Fig.13 Intercomparison of S_1

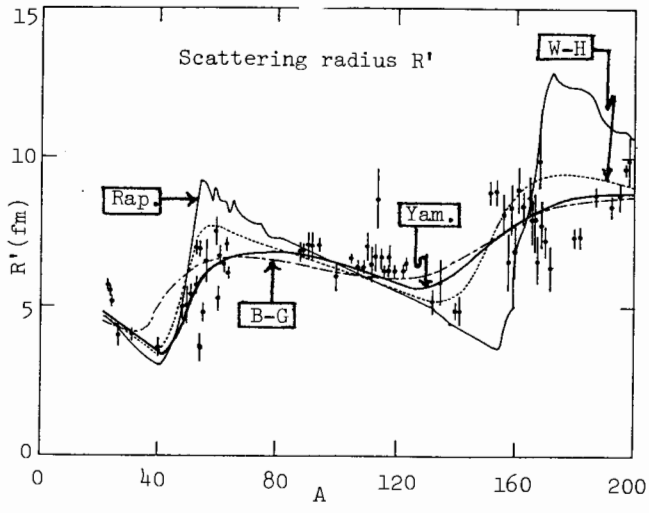

Fgi.14 Intercomparison of R'